Regional locus coeruleus degeneration is uncoupled from noradrenergic terminal loss in Parkinson's disease

Christopher E. J. Doppler,[1,2] Martin B. Kinnerup,[3] Corinna Brune,[2] Ezequiel Farrher,[4] Matthew Betts,[5,6,7] Tatyana D. Fedorova,[3] Jeppe L. Schaldemose,[3] Karoline Knudsen,[3] Rola Ismail,[3] Aline D. Seger,[1,2] Allan K. Hansen,[3] Kristian Stær,[3] Gereon R. Fink,[1,2] David J. Brooks,[3,8,9] Adjmal Nahimi,[3] Per Borghammer[3,†] and Michael Sommerauer[1,2,3,†]

[†]**These authors contributed equally to this work.**

Abstract

Previous studies have reported substantial involvement of the noradrenergic system in Parkinson's disease. Neuromelanin-sensitive MRI sequences and PET tracers have become available to visualize the cell bodies in the locus coeruleus and the density of noradrenergic terminal transporters. Combining these methods, we investigated the relationship of neurodegeneration in these distinct compartments in Parkinson's disease. We examined 93 subjects (40 healthy controls and 53 Parkinson's disease patients) with neuromelanin-sensitive turbo spin-echo MRI and calculated locus coeruleus-to-pons signal contrasts. Voxels with the highest intensities were extracted from published locus coeruleus coordinates transformed to individual MRI. To also investigate a potential spatial pattern of locus coeruleus degeneration, we extracted the highest signal intensities from the rostral, middle, and caudal third of the locus coeruleus. Additionally, a study-specific probabilistic map of the locus coeruleus was created and used to extract mean MRI contrast from the entire locus coeruleus and each rostro-caudal subdivision. Locus coeruleus volumes were measured using manual segmentations. A subset of 73 subjects had ^{11}C-MeNER PET to determine noradrenaline transporter density, and distribution volume ratios of noradrenaline transporter-rich regions were computed. Parkinson's disease patients showed reduced locus coeruleus MRI contrast independently of the selected method (voxel approaches: $p < 0.0001$, $p < 0.001$; probabilistic map: $p < 0.05$), specifically on the clinically-defined most affected side ($p < 0.05$), and reduced locus coeruleus volume ($p < 0.0001$). Reduced MRI contrast was confined to the middle and caudal locus coeruleus (voxel approach – rostral: $p = 0.48$, middle: $p < 0.0001$, and caudal: $p < 0.05$; probabilistic map – rostral: $p = 0.90$, middle: $p < 0.01$, and caudal: $p < 0.05$). The noradrenaline transporter density was lower in Parkinson's disease patients in all

examined regions (group effect $p < 0.0001$). No significant correlation was observed between locus coeruleus MRI contrast and noradrenaline transporter density. In contrast, the individual ratios of noradrenaline transporter density and locus coeruleus MRI contrast were lower in Parkinson's disease patients in all examined regions (group effect $p < 0.001$). Our multimodal imaging approach revealed pronounced noradrenergic terminal loss relative to cellular locus coeruleus degeneration in Parkinson's disease; the latter followed a distinct spatial pattern with the middle-caudal portion being more affected than the rostral part. The data shed first light on the interaction between the axonal and cell body compartments and their differential susceptibility to neurodegeneration in Parkinson's disease, which may eventually direct research toward potential novel treatment approaches.

Author affiliations:

1 Institute of Neuroscience and Medicine (INM-3), Forschungszentrum Jülich, D-52425 Jülich, Germany
2 University of Cologne, Faculty of Medicine and University Hospital Cologne, Department of Neurology, D-50937 Köln, Germany
3 Department of Nuclear Medicine and PET, Aarhus University Hospital, DK-8200 Aarhus N, Denmark
4 Institute of Neuroscience and Medicine (INM-4), Forschungszentrum Jülich, D-52425 Jülich, Germany
5 German Center for Neurodegenerative Diseases (DZNE), D-39120 Magdeburg, Germany
6 Institute of Cognitive Neurology and Dementia Research, Otto-von-Guericke-University Magdeburg, D-39120 Magdeburg, Germany
7 Center for Behavioral Brain Sciences, University of Magdeburg, D-39120 Magdeburg, Germany
8 Division of Brain Sciences, Imperial College London, London SW7 2AZ, UK
9 Institute of Translational and Clinical Research, University of Newcastle upon Tyne, Newcastle upon Tyne NE1 7RU, UK

Correspondence to: Michael Sommerauer, MD
Department of Neurology, University Hospital Cologne, Faculty of Medicine, University of Cologne, Kerpener Straße 62, D-50937 Köln, Germany
E-mail: michael.sommerauer@uk-koeln.de

Running title: Uncoupled noradrenergic degeneration

Keywords: Parkinson's disease; noradrenaline; MeNER; positron emission tomography; neuromelanin

Abbreviations: ^{11}C-MeNER = (2R)-2-[(S)-(2-(111C)methoxyphenoxy)phenylmethyl]-morpholine; ANTs = Advanced Normalization Tools; DVR = distribution volume ratio; FAST = FMRIB's Automated Segmentation Tool; FLIRT = FMRIB's Linear Image Registration Tool; FSL = FMRIB Software Library; HC = healthy control; LC = locus coeruleus; LEDD = levodopa-equivalent daily doses; MoCA = Montreal Cognitive Assessment; MDS = Movement Disorder Society; MNI = Montreal Neurological Institute; UPDRS = Unified Parkinson's disease Rating Scale; TSE = turbo spin-echo; VOI = volume of interest

Introduction

The locus coeruleus (LC) is the primary source of noradrenergic innervation in the brain and comprises clusters of 30,000-50,000 pigmented neurons located bilaterally in the dorsal pons.[1–4] The pigmentation of the LC (and that of the substantia nigra) is due to accumulating neuromelanin, a byproduct of catecholaminergic neurotransmitter metabolism, which forms paramagnetic complexes with iron.[5]

Despite the small size of the LC, i.e., about 15 mm^3, its axons are highly arborized,[6] providing numerous cortical and subcortical connections.[7] Consequently, the LC is involved in modulating many physiological processes, including sleep-wake regulation, attention and arousal, cognition, pain, blood-pressure regulation, and neuroinflammation.[8–13] Noradrenergic dysfunction has been reported in both Parkinson's disease and Alzheimer's disease.[3,14–16] Neuropathological studies have identified the LC as particularly susceptible to pathology, and its degeneration may occur early during both Alzheimer's disease and Parkinson's disease.[14,17]

Recent advances in neuroimaging allow investigating different compartments of the noradrenergic system *in vivo*. Using neuromelanin-sensitive MRI sequences, the paramagnetic pigment in the LC cell bodies can be visualized.[1,18] Given the reduction of this signal in patients with Alzheimer's disease and Parkinson's disease,[19,20] neuromelanin can be considered a potential biomarker for LC cell body integrity.[21] Efferent noradrenergic projections have also been shown to degenerate in Parkinson's disease. Their terminals can be visualized using PET with ^{11}C-MeNER, a reboxetine analogue that binds specifically to noradrenaline transporters located at the terminal sites.[15,16,22,23]

It remains to be investigated how terminal degeneration relates to LC neuronal cell loss in Parkinson's disease. Evidence from the dopaminergic system suggests that striatal terminal pathology precedes and exceeds degeneration of nigral cell bodies in Parkinson's disease, supporting a "dying-back" mechanism of neurodegeneration.[24–27] This mechanism of axonal pathology may well be common to degeneration of other monoaminergic neurotransmitter systems and the topographic organization of the LC could have implications for a disease-specific pattern of neuronal degeneration as neurons in the rostral LC project to the forebrain including the hippocampus, whereas those located in its middle and caudal portions project to the basal ganglia, cerebellum, and spinal cord.[28–31] In support of this view, histopathological studies in Alzheimer's disease and Parkinson's disease suggest that cellular degeneration of the LC might follow a disease-specific rostro-caudal pattern. The caudal part of the LC, which seems to be spared from

neurodegeneration in Alzheimer's disease,[20] is prone to neurodegeneration in Parkinson's disease.[32]

We hypothesized a distinct spatial pattern of LC disintegration with more significant degeneration of its caudal than its rostral portion in Parkinson's disease patients as visualized by neuromelanin-sensitive MRI. Concerning the relationship of LC cell body degeneration and terminal dysfunction, we predicted a pronounced noradrenergic terminal loss in Parkinson's disease consistent with an uncoupling between terminals and axons. To this end, we analyzed 93 datasets of Parkinson's disease patients and healthy controls (HC) who had undergone multimodal imaging combining neuromelanin-sensitive MRI and ^{11}C-MeNER PET.

Materials and methods

Study design and participants

We pooled data from two studies on Parkinson's disease from Aarhus University, in which we conducted ^{11}C-MeNER PET and neuromelanin-sensitive MRI.[15] In total, 40 HC and 53 Parkinson's disease patients had neuromelanin-sensitive MRI assessments and were eligible for analysis. Of those, a subgroup of 26 HC and 47 Parkinson's disease patients also had ^{11}C-MeNER PET imaging. Inclusion criteria comprised a diagnosis of Parkinson's disease according to the Movement Disorder Society (MDS) consensus criteria,[33] a Montreal Cognitive Assessment (MoCA) score greater than 22, and a normal structural brain MRI scan. Exclusion criteria were dementia, psychiatric disorders including depression operationalized by an increased score on the Geriatric Depression Scale (GDS-15), neurological disorders besides Parkinson's disease, and medication interfering with the noradrenaline transporters, particularly selective serotonin-noradrenaline reuptake inhibitors and tricyclic antidepressants. Inclusion and exclusion criteria were identical for HC apart from a diagnosis of Parkinson's disease. One patient was treatment-naïve. The other patients were either taking levodopa, dopamine agonists, MAO B inhibitors, or a combination thereof. Total levodopa-equivalent daily doses (LEDD) were calculated as recommended.[34] Motor symptoms were quantified after 12 hours of medication abstinence: in a subset of 25 patients, the Unified Parkinson's disease Rating Scale part III (UPDRS III) was applied; for the other 28 patients, the updated MDS-UPDRS III was used. To facilitate comparisons, the older UPDRS III

values were converted to match with the MDS-UPDRS III system using the approach suggested by the MDS.[35]

Asymmetry of Parkinson's disease motor symptoms was assumed if (1) the difference of UPDRS right- minus left-side items was ≥4 and (2) matched the side of onset. Otherwise, laterality was considered as indifferent.[36] For statistical analysis, the "most affected side" of the LC was the side contralateral to the body side with higher motor burden, i.e. ipsilateral to the greatest nigrostriatal denervation.

All subjects were recruited through advertisements in newspapers and the Danish Parkinson's disease magazine, and collaborating neurological clinics. Following the Declaration of Helsinki, the local ethics committee approved the study, and all subjects gave written informed consent.

Neuromelanin-sensitive MRI

We acquired 2D axial turbo spin-echo (TSE) T1-weighted sequences in all subjects. Due to limited scanner availability, subjects were scanned on two scanners with slightly different scanning protocols: 46 subjects (18 HC and 28 Parkinson's disease patients) were scanned on a Siemens MAGNETOM Trio using a 32-channel head coil (repetition time/echo time: 600 ms/10 ms, 16 averages, voxel size: 0.4 × 0.4 × 1.8 mm^3, distance factor 10%), and 47 subjects (22 HC and 25 Parkinson's disease patients) were scanned on a Siemens MAGNETOM Prisma using a 32 channel head coil (repetition time/echo time: 825 ms/18 ms, 16 averages, voxel size: 0.4 × 0.4 × 1.8 mm^3, distance factor 10%). Populations from both scanners did not differ regarding age, sex, and Montreal Cognitive Assessment (MoCA) scores (all $p > 0.05$). Due to ethical reasons and to reduce movements within the scanner, which would particularly be problematic for imaging small brainstem structures like the LC, Parkinson's disease patients were scanned in medication ON state. There is evidence from animal studies that administration of levodopa might foster the accumulation of neuromelanin.[37] However, these effects are expected to be relatively long-lasting rather than fluctuating between medication states.

Planes were acquired perpendicular to the dorsal brainstem. To account for inhomogeneities in the transmit/receive coil profiles of the different scanners, TSE images were bias field-corrected using FMRIB's Automated Segmentation Tool (FAST)[38] available in the FMRIB Software Library v6.0 (FSL).[39] As it is currently unclear how the approach for quantifying neuromelanin MRI contrast in the LC may influence results,[21] we used two complementary approaches: (A) delineation of voxels

with the highest intensity within bilateral larger "LC searching volumes of interest (VOIs)", comparable to previously published LC quantifications in Parkinson's disease,[15,16,40,41] and (B) creation of a probabilistic map of the LC within a study-specific template to quantify mean LC MRI contrast as described in recent aging and Alzheimer's disease studies (Fig. 1).[2,4,42]

Approach A was carried out using toolboxes in PMOD 4.0: Published contours of the LC in Montreal Neurological Institute (MNI) atlas space[1] were slightly enlarged to "LC searching VOIs" that included the LC but no other structure with similarly high contrast on the TSE image. To investigate rostro-caudal differences in LC contrast, the aforementioned "LC searching VOIs" were additionally split into three parts of an equal rostro-caudal length in PMOD. A rectangular background VOI was centered in the pons. The MNI atlas VOIs were co-registered to the individual TSE images for each subject using combined inverse transformations from MNI atlas space to anatomical T1 (derived from spatial normalization of the segmented T1 image to MNI space) and from anatomical T1 to the TSE image (derived from a rigid transformation of the TSE to the T1 image) allowing for image analysis in native space. Following previous studies, the 12 connected voxels with the highest intensity,[41] and the 10 independent voxels with the highest intensity[15] in each "LC searching VOI" were identified by the appropriate VOI tools implemented in PMOD 4.0. The average intensities of the resulting voxels for each side were divided by the background intensity of the pontine VOI. With a similar approach, we identified the 5 independent voxels with the highest intensity in each rostro-caudal section of the "LC searching VOIs", averaged the resulting voxels' intensities, and divided these by the background intensity of the pontine VOI.

For approach B, we first created a study-specific probabilistic map of the LC. To this end, TSE images were first *sinc*-interpolated to a near isotropic voxel size of $0.4 \times 0.4 \times 0.5$ mm^3 with PMOD 4.0. On these images, two trained raters manually segmented the LC as hyperintense voxels on either side of the dorsal pons adjacent to the fourth ventricle with ITK-SNAP.[43] To enable co-registration of all TSE images to a study-specific template space, images were padded with 50 voxels in all dimensions, and a common template was created using the "buildtemplateparallel" command from Advanced Normalization Tools (ANTs v2.1).[44] Warping of the images to template space failed in seven subjects using this approach. Three of those images were successfully warped using FLIRT and FNIRT in FSL.[39] The remaining four subjects had to be excluded from the analysis. Manual LC segmentations were transferred to the study-specific template space using the transformations generated during template creation. Segmentations of HC subjects in template

space were averaged, which yielded a probability of each voxel belonging to the LC. By computing a cumulative distribution function of the map and selecting the range for which this function approximated a linear distribution, a threshold for map binarization was empirically set at a minimum voxel probability of 22%.[45] This step mitigated the potential effects of inaccuracies in manual segmentation and coregistration.[45] The binarized map was multiplied with each TSE image in the study-specific template space to mask the LC. Mean voxel intensities were extracted using fslmaths and divided by the average intensity of a rectangular pontine background VOI drawn in the template space. To enable computation of rostro-caudal differences in LC MRI contrast consistent with approach A, the binarized map was again split into three parts of equal rostro-caudal length along the z-axis. As another surrogate parameter for LC, we extracted the cumulative bilateral volume of the individual segmentations of HC and Parkinson's disease patients in native space. Image analysis steps are summarized in Fig. 1.

^{11}C-MeNER PET

^{11}C-MeNER radiosynthesis and PET image acquisition and reconstruction were performed as described previously.[22] After bolus administration of ^{11}C-MeNER, a 90-minute dynamic PET scan was acquired with an ECAT HRRT. All PET images were analyzed using the relevant toolboxes of PMOD 4.0. Image frames were rigidly realigned to an average image acquired 5-10 minutes after injection for motion correction. Corrected PET images were spatially normalized into MNI space with individual MRI segmentation-based transformation and rigid matching of the PET image to the corresponding anatomical MRI. We smoothed PET images with a 4 mm Gaussian filter to optimize voxel-wise kinetic modeling. VOIs of the bilateral thalamus (high-binding) and caudate (low-binding) from PMOD's built-in atlas were used to start pixel-wise calculations using the reference tissue model 2 (SRTM2) with a fixed efflux rate constant $k2' = 0.021*min^{-1}$ to obtain ^{11}C-MeNER parametric maps of distribution volume ratios (DVRs) comparable to previous studies.[15,16] These maps were non-rigidly matched to an in-house ^{11}C-MeNER template comprising six VOIs rich in noradrenaline transporters: the hypothalamus (left/right), red nucleus (left/right), median raphe, and dorsal raphe (Supplementary Fig. 1). Inverse transformations were applied to these VOIs. Furthermore, additional VOIs for the thalamus (left/right) from PMOD's built-in atlas were included. DVRs of these VOIs were extracted for further statistical analysis.

Statistical analysis

We interrogated the data using RStudio (Version 1.3.959) and packages "lme4"[46] and "emmeans".[47] Data distribution was assessed with Shapiro-Wilk tests, Q-Q plots, and density plots. Group data are presented as mean ± standard deviation unless otherwise stated.

Linear mixed models were used to interrogate the different analytical approaches for PET and MRI data separately. Models were constructed using a step-up strategy, starting with an intercept-only model and incrementally adding predictors. As ^{11}C-MeNER DVRs and LC designations did not differ between sides (all $p > 0.05$), we averaged sides for inter-group comparison to reduce the number of statistical comparisons across groups.

For the linear mixed model analyzing MRI data covering the full LC, "LC MRI contrast" was used as the outcome variable. Factors "group" (HC, Parkinson's disease) and "method" (12 connected voxels with the highest intensity, 10 independent voxels with the highest intensity, mean intensity in the probabilistic map) were considered as fixed effects and "subject" as random effect. Due to a considerable numeric difference of volume measures compared to voxel intensities, LC volumes were interrogated with a separate linear model. To investigate the rostro-caudal spatial distribution of LC MRI contrast, the respective linear mixed model was expanded using "region" (rostral, middle, caudal) as a fixed effect. "Method" as another fixed effect, in this case, was represented by the two different approaches (5 independent voxels with the highest intensity, mean intensity in the probabilistic map). For linear mixed models assessing laterality in LC MRI contrasts, "side" (most and least affected) was considered as a fixed effect.

For PET data, the final model encompassed "Distribution Volume Ratios" as outcome variable, "region" (representing the different PET VOIs) and "group" (HC, Parkinson's disease) as fixed effects, and "subject" as a random effect.

To investigate the relationship between noradrenaline transporter density and LC MRI contrast, we calculated intra-individual ratios of DVR to LC MRI contrast. For each region investigated, ratios were normalized to the mean of the HC group (i.e., leading to a group mean of 1 for HC for each region). The linear mixed model was constructed analogously to the PET data analysis with "scanner type" as an additional fixed effect.

"Scanner type" was included as a fixed effect in all models, and its partial correlation was determined for all correlation analyses interrogating MRI contrasts to control for potential bias due to different TR/TE values. Besides, gender, age, and MoCA scores were controlled for in all models

and correlation analyses. Visual inspection of residual plots did not reveal any apparent deviations from homoscedasticity or normality. Estimated marginal means were calculated for *post-hoc* comparisons.

Further group comparisons were performed using Welch's *t*-tests, Mann-Whitney tests, and chi-square tests as appropriate. Significance was accepted at $p<0.05$. Correlations were computed with Pearson's correlation coefficient, and a Bonferroni-correction was applied due to the multiple comparisons: significance was accepted at $p_{adj} < \frac{0.05}{number\ of\ comparisons}$.

Data availability

Data are available upon reasonable request.

Results

Groups did not differ in mean age (range: 51 - 83.5 years), but the Parkinson's disease group included more males than the HC group (Table 1). The subgroup of HC subjects and Parkinson's disease patients who underwent MRI and PET imaging had a similar age/sex distribution and clinical characteristics compared to the entire sample (Table 1). The average MoCA score was lower in Parkinson's disease patients than in HC (27.8 ± 2.1 versus 26.6 ± 2.2, $p = 0.016$) but was still above the cut-off of 26 for Mild Cognitive Impairment (MCI) in Parkinson's disease.[48]

Investigating MRI contrast along the full extent of the LC, Parkinson's disease patients showed a lower contrast compared with HC subjects with every analytical method (β = -0.04; effect of "group": $F(1, 80.313) = 14.74$, $p < 0.001$; $\eta_p^2 = 0.16$) with absolute values varying between methods (effect of "method": $F(2, 164.621) = 1870.47$, $p < 0.0001$; $\eta_p^2 = 0.96$; Fig. 2). Group differences between HC and Parkinson's disease patients were more pronounced for the approaches investigating the 12 connected voxels ($t(111) = 4.80$, $p < 0.0001$; $d = 2.13$) and the 10 independent voxels with the highest intensity ($t(111) = 3.58$, $p < 0.001$; $d = 1.58$) but were still significant when comparing the mean intensity of the probabilistic map ($t(114) = 2.18$, $p < 0.05$; $d = 0.97$) (interaction "group" × "method": $F(2, 164.610) = 6.86$, $p < 0.01$; $\eta_p^2 = 0.08$). Parkinson's disease patients also exhibited a lower LC volume than HC (β = -3.61; effect of "group": $F(1, 80) = 30.03$, $p < 0.0001$; $\eta_p^2 = 0.27$). All quantifications of LC contrast besides LC volume showed significant positive inter-method correlations (all $r \geq 0.6$, all $p < p_{adj}$ (0.05/6 = 0.008), Supplementary Fig. 2).

Analyzing the rostro-caudal distribution of LC MRI contrast, Parkinson's disease patients exhibited reduced contrast in the middle (β = -0.03) and caudal (β = -0.01) but not the rostral sections of the LC compared to HC (effect of "position": $F(2, 408.94 = 60.33)$, $p < 0.0001$; $\eta_p^2 = 0.23$; interaction "group" × "position": $F(2, 408.94 = 7.48$, $p < 0.001$; $\eta_p^2 = 0.04$; Fig. 3). Both methods used to analyze the spatial distribution of the contrast along the rostro-caudal axis revealed similar results (probabilistic map - HC versus Parkinson's disease, rostral: $t(308) = 0.13$, $p = 0.900$; $d = 0.03$, middle: $t(308) = 2.70$; $p < 0.01$, $d = 0.74$, caudal: $t(308) = 2.57$, $p < 0.05$; $d = 0.70$, Fig. 3A; voxel approach - HC versus Parkinson's disease, rostral: $t(298) = 0.71$, $p = 0.476$; $d = 0.19$, middle: $t(298) = 4.33$, $p < 0.0001$; $d = 1.16$, caudal: $t(298) = 2.20$, $p < 0.05$; $d = 0.59$, Fig. 3B). Absolute values returned by the different methods also differed significantly (effect of "method": $F(1, 414.68) = 1939.67$, $p < 0.0001$; $\eta_p^2 = 0.82$); however, contrast values for each rostro-caudal section were positively correlated across methods (all $r > 0.3$, all $p < p_{adj}$ (0.05/3 = 0.017)). LC

MRI contrasts did not differ between the clinically-defined most and least affected side when interrogating the entire probabilistic map (effect of "side": $F(1,24) = 3.84$, $p = 0.06$; $\eta_p^2 = 0.14$; Fig. 4A) but its sections along the rostro-caudal axis (effect of "side": $F(1,120) = 4.35$, $p < 0.05$; $\eta_p^2 = 0.03$; Fig. 4B). *Post-hoc* comparisons revealed lower contrast specifically for the middle sections of the most affected side ($t(120) = 2.25$, $p < 0.05$; $d = 0.63$).

^{11}C-MeNER DVRs were significantly lower in Parkinson's disease patients compared to HC across all noradrenaline transporter rich regions ($\beta = -0.15$; effect of "group": $F(1,65) = 22.84$, $p < 0.0001$; $\eta_p^2 = 0.26$, pontine raphe: $t(224) = 2.80$, $p < 0.01$; $d = 0.85$, dorsal raphe: $t(224) = 4.32$, $p < 0.0001$; $d = 1.32$, red nucleus: $t(224) = 3.31$, $p < 0.01$; $d = 1.01$, hypothalamus: $t(224) = 3.60$, $p < 0.001$; $d = 1.10$, thalamus: $t(224) = 2.42$, $p < 0.05$; $d = 0.74$; interaction "group" × "region" $F(4,272) = 0.81$, $p = 0.519$; $\eta_p^2 = 0.01$; Fig. 5).

In Parkinson's disease patients, noradrenaline transporter density across all five regions sampled showed no correlation with LC MRI contrast along the full extent of the LC regardless of which of the four methods was used (all $p > 0.3$, all $|r| < 0.16$, $p_{adj} = 0.05/20 = 0.0025$; Fig. 6 and Supplementary Fig. 3A). There was also no association between noradrenaline transporter density and MRI contrast measures along the rostro-caudal axis of the (all $p > 0.02$, all $|r| < 0.35$, $p_{adj} = 0.05/30 = 0.0006$, Supplementary Fig. 3B). Partial correlations with age, gender, and MoCA score were accounted for by both correlation analyses. There was no linear association with disease duration for both LC MRI contrast and noradrenaline transporter density (Supplementary Fig. 4).

To further investigate the relationship between noradrenaline transporter density and LC MRI contrast in Parkinson's disease patients, we calculated ratios of ^{11}C-MeNER PET DVR to LC MRI contrast. For each region investigated, the individual ratio was normalized to the mean of the HC, i.e., a ratio below 1 indicated that noradrenaline transporter density loss exceeded LC MRI contrast deprivation. This was the case for Parkinson's disease patients as they showed a significantly lower ratio compared to HC ($\beta = -0.07$; effect of "group": $F(1,61) = 14.69$, $p < 0.001$; $\eta_p^2 = 0.19$). This reduction was between 7 and 12 % when using the LC contrast defined from the probabilistic map, and consistent for all regions (pontine raphe: $t(193) = 1.99$, $p < 0.05$; $d = 0.64$, dorsal raphe: $t(193) = 3.45$, $p < 0.001$; $d = 1.11$, red nucleus: $t(193) = 2.58$, $p < 0.05$; $d = 0.83$, hypothalamus: $t(193) = 3.56$, $p < 0.001$; $d = 1.15$, thalamus: $t(193) = 2.10$, $p < 0.05$; $d = 0.68$; effect of "region" and interaction "group" × "region": both $F(4,260) = 0.88$; $p = 0.474$; $\eta_p^2 = 0.01$, Fig. 7). The same held true when using the two voxel-based LC MRI contrast measures where reductions between 15 -

22% were observed (10 independent voxels with highest intensity - $\beta = -0.18$; effect of "group": $F(1,64) = 78.81$, $p < 0.0001$; $\eta_p^2 = 0.55$, effect of "region" & interaction "group" × "region": $F(4,272) = 0.67$, $p = 0.611$; $\eta_p^2 = 0.01$, pontine raphe: $t(209) = 5.66$; $d = 1.77$, dorsal raphe: $t(209) = 6.90$; $d = 2.15$, red nucleus: $t(209) = 6.09$; $d = 1.90$, hypothalamus: $t(209) = 7.00$; $d = 2.18$, thalamus: $t(209) = 5.67$; $d = 1.77$, all regions: $p < 0.0001$; 12 connected voxels with highest intensity: $\beta = -0.16$; effect of "group": $F(1,64) = 60.09$, $p < 0.0001$; $\eta_p^2 = 0.48$, effect of "region" & interaction "group" × "region": $F(4,272) = 0.69$, $p = 0.597$; $\eta_p^2 = 0.01$, pontine raphe: $t(212) = 4.82$; $d = 1.50$, dorsal raphe: $t(212) = 6.09$; $d = 1.89$, red nucleus: $t(212) = 5.26$; $d = 1.63$, hypothalamus: $t(212) = 6.18$; $d = 1.92$, thalamus: $t(212) = 4.83$; $d = 1.50$, all regions: $p < 0.0001$).

Discussion

We assessed two compartments of the noradrenergic system using multimodal *in vivo* imaging in a large sample of healthy controls (HC) and Parkinson's disease patients: the terminals with ^{11}C-MeNER PET - specific for noradrenaline transporters - and the cell bodies with TSE MRI - sensitive to neuromelanin content. Parkinson's disease patients showed a highly significant decrease of both imaging markers consistent with *postmortem* and *in vivo* data on noradrenergic perturbations in Parkinson's disease.[15,23,32,41,49–52] Applying fine-mapping of the LC MRI contrast along its rostro-caudal axis revealed a distinct spatial pattern of LC degeneration in Parkinson's disease in the middle and caudal LC with relative sparing of the rostral third. Decreased LC MRI contrast was pronounced for the middle section of the clinically-defined most affected side. We also studied the association of these markers of noradrenergic terminal function and LC cell body integrity but did not find a linear correlation. Instead, terminal deterioration measured with ^{11}C-MeNER PET exceeded cell body disintegration measured with neuromelanin-sensitive MRI by 10 - 20%, suggesting predominant terminal damage of the noradrenergic system in Parkinson's disease.

Uncoupled degeneration of terminals and cell bodies in Parkinson's disease

An increasing body of evidence - mainly deduced from studies of the dopaminergic system - indicates axonal degeneration as a central part of Parkinson's disease pathology, which is differentially regulated from cell body death.[24,25,53–55] It is well-recognized that Parkinson's disease pathology preferentially affects neuronal populations possessing long and hyperbranched axons, including dopaminergic nigrostriatal neurons, cholinergic neurons of the pedunculopontine nucleus and the dorsal motor nucleus of the vagus, as well as noradrenergic neurons in the LC.[17,56,57] Estimates of the terminal fields proposed that one dopaminergic neuron from the substantia nigra is connected to up to 75000 striatal neurons,[58] and a similar large arborization of projections is reported for LC neurons.[59] It seems probable that maintenance of such a complex structure of axonal arborization leads to high energetic costs to the neuron, and cellular insults arising from, e.g., the abnormal α-synuclein aggregation characterizing Parkinson's disease will have a substantial impact on the particularly elaborate axonal compartment.

Surprisingly, comparative histopathological studies of the terminals and cell bodies in Parkinson's disease remain scarce. Kordower and colleagues[60] examined 28 brains of Parkinson's disease patients at various disease stages and reported an uncoupling of degenerative processes in the dopaminergic system. There was a severe decrease of optic density of tyrosine hydroxylase and dopamine transporter positive axons in the striatum in early Parkinson's disease, which then stabilized. In contrast, neuromelanin and tyrosine hydroxylase positive cells at the level of the substantia nigra showed only mild reductions with more significant declines in later disease stages.[60] These results are supported by a meta-analysis performed by Cheng and colleagues.[24] They concluded that at the time of Parkinson's disease diagnosis, dopamine terminal loss in the striatum exceeds cell body loss in the substantia nigra by a similar percentage to that revealed in our study - and that this phenomenon persists in later stages.[24] Moreover, in Parkinson's disease animal models, including rodents and primates, utilizing various toxic injuries and genetic modifications, terminal dysfunction typically precedes and exceeds cellular death in the dopaminergic system.[26,61–65] Aggregates of pathological α-synuclein can directly interfere with intracellular transport mechanisms, including trafficking along the axon to the terminals, resulting in impaired communication and homeostatic regulation from the cell body, eventually uncoupling the two compartments.[66] In Parkinson's disease, the dopaminergic and noradrenergic neurons might be considered 'sick-but-not-dead', as proposed by Goldstein.[67] Thus, surviving cells still incorporate neuromelanin pigment in their somata while showing severe functional impairment leading to a significantly trimmed axonal arborization described as 'dying-back'.[24]

To the best of our knowledge, this is the first multimodal comparative *in-vivo* imaging study assessing the relationship between markers of noradrenergic terminals and cell bodies in Parkinson's disease patients. Our data are comparable to previous reports of the dopaminergic system. In those studies, various techniques for quantifying dopaminergic terminals were used, including dopamine transporter ligands for single-photon emission computed tomography (SPECT)[55,68–72] and PET[73] as well as different quantifications of substantia nigra integrity, including neuromelanin-sensitive MRI,[69,72,73] off-target binding to neuromelanin by the tau PET marker flortaucipir,[55] and *postmortem* cell counts.[68,70,71] Three of the seven studies included mixed cohorts and combined Parkinson's disease patients with patient samples without a dopaminergic deficit.[69–71] These studies found a significant correlation between measures of somatic and terminal compartments but were driven by group effects of subjects with dopaminergic degeneration versus

subjects with an intact dopamine system. In studies restricted to patients with Parkinson's disease and other movement disorders with degeneration of the dopaminergic system, results turned out to be more heterogeneous. The majority of these studies showed no clear association between nigral neuromelanin and dopamine terminal function. Saari and colleagues[68] (including patients with multisystem atrophy, progressive supranuclear palsy, and Parkinson's disease and incorporating neuropathological assessment) and Hansen and colleagues[55] did not find a significant correlation between these parameters. In a recent study of Martín-Bastida *et al.,*[73] correlation of striatal dopamine transporter PET with substantia nigra neuromelanin-sensitive MRI was only seen in the clinically more affected side of Parkinson's disease patients. In contrast, Isaias *et al.*[72] reported a strong association. In comparison to the studies mentioned above, we investigated a sample more than twice as large using different approaches to quantify LC neuromelanin content. We assume that the combination of these factors leads to a high validity of our results.

Summarizing *postmortem* and *in vivo* results of the dopaminergic system in Parkinson's disease, these data do not support a clear linear linkage of degeneration of the terminal and cell body compartments. Relating the estimations of terminal deterioration, measured with ^{11}C-MeNER PET, and cell body disintegration, measured with neuromelanin-sensitive MRI, we conclude that pronounced axonal damage exceeds somatic damage of the noradrenergic system in Parkinson's disease.

Spatial pattern of LC degeneration

Even though the LC is tiny, comprising only tens of thousands of neurons, recent evidence suggests that it has a sophisticated spatial organization, allowing various physiological engagements.[6,7] A modern view of the LC presumes that it encompasses a complex combination of converging and diverging afferents and efferents. Some of its afferents innervate a substantial fraction of the LC, permitting generalized activation of the entire nucleus, while other afferents display highly specific cell-to-cell connections and activate only selected neurons.[74] Similarly, some of its efferent connections project to many brain regions and others to discrete terminal fields.[75] More complexity is added when these two different connectivity patterns coincide within the same cell in the LC.[7] This particular microstructure of the LC is a crucial factor distinguishing the noradrenergic from the dopaminergic nigro-striatal system in which striatal terminal fields of nigral regions show a

relatively fixed spatial arrangement.[45,76] Hence, comparison of LC cell density (as potentially measured with neuromelanin-sensitive MRI of the LC) and noradrenergic terminals in different brain regions (as investigated with noradrenaline transporter PET) might only be the first step to assess the relation of these compartments of the noradrenergic system *in vivo*.

The notion of a defined LC microstructure is supported by accumulating evidence of focal changes caused by neurodegenerative diseases. In a seminal study from 1992, German and colleagues[32] reported disease-specific patterns of LC neurodegeneration. Parkinson's disease patients exhibited cell loss targeting the caudal parts of the LC, whereas Alzheimer's disease patients (and subjects with Down's syndrome) showed a sparing of this subregion.[32] Sparing of the caudal LC was recently replicated using neuromelanin-sensitive MRI in Alzheimer's disease patients at various disease stages.[20] The rostral LC would appear to have a role in mediating memory performance based on LC MRI findings.[4] We found reduced MRI contrast specifically in the caudal parts of the LC but relative sparing of the rostral parts in our cognitively intact Parkinson's disease sample. Whether Parkinson's disease patients with significant memory deficits show reduced MRI contrast in the rostral LC section too warrants future investigation.[77]

Recent studies have shown associations between neuromelanin content of the substantia nigra and clinical features of Parkinson's disease like laterality.[45,73] We extend these findings by presenting first evidence for an association between a disintegration of the LC and motor symptom side, suggesting that the LC and the substantia nigra show the greatest level of degeneration on the same side of the brainstem. This finding was predicted by the recently proposed "α-synuclein Origin and Connectome Model (SOC Model)", which provides a framework particularly for the laterality of motor (and non-motor) symptoms in Parkinson's disease. [78]

Technical remarks on LC MRI quantification

The most appropriate method for quantifying neuromelanin-sensitive MRI signals from the LC has not yet been agreed[21], and its optimal localization is still debated.[79,80] In Parkinson's disease, more than half a dozen different quantification approaches have been suggested, although these methods converge with regard to normalizing LC MRI contrast to a reference region in adjacent pontine tissue. We, therefore, tested four different approaches of LC delineation, including contrast-based and volumetric measures as well as atlas-based and manual approaches. All quantifications

provided comparable results between groups and were highly correlated with each other, suggesting that the choice of method did not significantly impact our findings.

Limitations

We used two different quantifications to estimate the integrity of each cellular compartment and cannot rule out unequal contrast behaviors of PET and MRI, e.g., due to differential sensitivities of these approaches. This is an intrinsic issue for all multimodal (imaging) studies, which also relates to comparisons of *antemortem* imaging data and *postmortem* quantifications. However, several studies have reported that LC MRI contrast is concordant with histological assessments of LC integrity.[1,3,20,86] *In vitro* studies with autoradiography and blocking studies have shown highly specific binding of ^{11}C-MeNER to noradrenaline transporters confirming its ability to quantify the transporter density with PET imaging validly.[87–89]

Another limitation is that we merged two MRI datasets acquired with different scanners and scanning protocols. This approach might have increased the variance across groups. However, samples were comparable concerning the subjects recruited and their demographic characteristics. Additionally, the scanner type was set as a covariate in all statistical models. Extending the correlation analysis by partial correlations with different scanner types did also not change the results significantly.

Investigating the association between non-motor symptoms and the integrity of different compartments of the noradrenergic system would be of great interest. For the two independent data sets using multimodal imaging of the noradrenergic system that were pooled for this study, no homogenous evaluation of non-motor symptoms was available. Still, we have considered significant deviations in GDS-15 and MoCA scores as exclusion criteria. Parkinson's disease patients had a lower MoCA score compared to healthy controls. This finding might be expected as our sample of Parkinson's disease patients had a mean disease duration of five years. We considered individual MoCA scores as a covariate in all statistical models and in the correlation analyses to account for this potential confound. For a detailed investigation of the association of non-motor symptoms and imaging parameters of the noradrenergic system, a systematic variation of these factors between groups would be needed. However, this question cannot be sufficiently addressed with our sample.

Our data are compatible with a "dying-back" pattern within the noradrenergic system, a pattern that has also been proposed for the dopaminergic system in neurodegenerative diseases. However, other mechanisms, e.g. adaptive processes of the noradrenaline transporters increasing synaptic availability of noradrenaline, might play a role and warrant further investigation.

Conclusions

Using a multimodal imaging approach combining ^{11}C-MeNER PET and neuromelanin-sensitive MRI, we found that the noradrenergic system shows a distinct pattern of degeneration in Parkinson's disease: more pronounced dysfunction of terminal compared to somatic structures (expressed as PET/MRI ratio) and preferential degeneration of the caudal compared to the rostral parts of the LC. Future studies, including comparisons of *in vivo* imaging findings with a histopathologic assessment of the different cellular compartments, are warranted to shed more light on the interaction between the axonal and cell body compartments and their differential susceptibility to Parkinson's disease neurodegeneration. Additionally, comparative studies in other neurodegenerative conditions like Alzheimer's disease might elucidate whether pronounced axonal damage is specific to Parkinson's disease or a fundamental principle of neurodegeneration. Such knowledge may direct research into potential novel treatment strategies specifically targeting the most affected structures.

Acknowledgements

We thank all study participants and Martin Hansov (University of Cologne) for his support in image analysis.

Funding

CEJD is supported by the Clinician Scientist Program (CCSP) / Faculty of Medicine / University of Cologne, funded by the Deutsche Forschungsgemeinschaft (DFG, German Research Foundation, FI 773/15-1)

MB is supported by the Deutsche Forschungsgemeinschaft (DFG, German Research Foundation) – Project-ID 425899996 – SFB 1436.

JLS is supported by the Clinical Medicine Programme / Faculty of Health / Aarhus University, funded by Olav Thon Foundation (project number AU259021).

MS is funded by the Danish Association of Parkinson's Disease (Parkinson-foreningen), the Swiss National Science Foundation (grant number P2SKP3_161812), the Hildegard Henssler-Stiftung, the Koeln Fortune Program / Faculty of Medicine, University of Cologne (grant number 453/2018), and the Else Kröner-Fresenius-Stiftung (grant number 2019_EKES.02)

GRF is funded by the Deutsche Forschungsgemeinschaft (DFG, German Research Foundation) – Project-ID 431549029 – SFB 1451.

PB is funded by the Lundbeck foundation (ID: R276-2018-294).

Competing interests

GRF serves as an editorial board member of Cortex, Neurological Research and Practice, NeuroImage: Clinical, Zeitschrift für Neuropsychologie, and DGNeurologie; receives royalties

from the publication of the books Funktionelle MRT in Psychiatrie und Neurologie, Neurologische Differentialdiagnose, and SOP Neurologie; received honoraria for speaking engagements from Bayer, Desitin, Ergo DKV, Forum für medizinische Fortbildung FomF GmbH, GSK, Medica Academy Messe Düsseldorf, Medicbrain Healthcare, Novartis, Pfizer, and Sportärztebund NRW.

Supplementary material

Supplementary material is available at *Brain* online.

References

1. Keren NI, Taheri S, Vazey EM, et al. Histologic validation of locus coeruleus MRI contrast in post-mortem tissue. *NeuroImage*. 2015;113:235-245. doi:10.1016/j.neuroimage.2015.03.020

2. Betts MJ, Cardenas-Blanco A, Kanowski M, Jessen F, Düzel E. In vivo MRI assessment of the human locus coeruleus along its rostrocaudal extent in young and older adults. *NeuroImage*. 2017;163:150-159. doi:10.1016/j.neuroimage.2017.09.042

3. Theofilas P, Ehrenberg AJ, Dunlop S, et al. Locus coeruleus volume and cell population changes during Alzheimer's disease progression: A stereological study in human postmortem brains with potential implication for early-stage biomarker discovery. *Alzheimer's & Dementia*. 2017;13(3):236-246. doi:10.1016/j.jalz.2016.06.2362

4. Dahl MJ, Mather M, Düzel S, et al. Rostral locus coeruleus integrity is associated with better memory performance in older adults. *Nat Hum Behav*. 2019;3(11):1203-1214. doi:10.1038/s41562-019-0715-2

5. Sulzer D, Cassidy C, Horga G, et al. Neuromelanin detection by magnetic resonance imaging (MRI) and its promise as a biomarker for Parkinson's disease. *npj Parkinson's Disease*. 2018;4(1):11. doi:10.1038/s41531-018-0047-3

6. Schwarz LA, Luo L. Organization of the Locus Coeruleus-Norepinephrine System. *Current Biology*. 2015;25(21):R1051-R1056. doi:10.1016/j.cub.2015.09.039

7. Poe GR, Foote S, Eschenko O, et al. Locus coeruleus: a new look at the blue spot. *Nat Rev Neurosci*. 2020;21(11):644-659. doi:10.1038/s41583-020-0360-9

8. Giorgi FS, Saccaro LF, Galgani A, et al. The role of Locus Coeruleus in neuroinflammation occurring in Alzheimer's disease. *Brain Research Bulletin*. 2019;153:47-58. doi:10.1016/j.brainresbull.2019.08.007

9. Cao S, Fisher DW, Yu T, Dong H. The link between chronic pain and Alzheimer's disease. *J Neuroinflammation*. 2019;16(1):204. doi:10.1186/s12974-019-1608-z

10. Rodovalho GV, Franci CR, Morris M, Anselmo-Franci JA. Locus Coeruleus Lesions Decrease Oxytocin and Vasopressin Release Induced by Hemorrhage. *Neurochem Res*. 2006;31(2):259-266. doi:10.1007/s11064-005-9015-5

11. Saper CB, Fuller PM, Pedersen NP, Lu J, Scammell TE. Sleep State Switching. *Neuron*. 2010;68(6):1023-1042. doi:10.1016/j.neuron.2010.11.032

12. Vazey EM, Aston-Jones G. The emerging role of norepinephrine in cognitive dysfunctions of Parkinson's disease. *Front Behav Neurosci*. 2012;6. doi:10.3389/fnbeh.2012.00048

13. Sugama S, Takenouchi T, Hashimoto M, Ohata H, Takenaka Y, Kakinuma Y. Stress-

induced microglial activation occurs through β-adrenergic receptor: noradrenaline as a key neurotransmitter in microglial activation. *J Neuroinflammation*. 2019;16(1):266. doi:10.1186/s12974-019-1632-z

14. Kelly SC, He B, Perez SE, Ginsberg SD, Mufson EJ, Counts SE. Locus coeruleus cellular and molecular pathology during the progression of Alzheimer's disease. A*cta neuropathol commun*. 2017;5(1):8. doi:10.1186/s40478-017-0411-2

15. Sommerauer M, Fedorova TD, Hansen AK, et al. Evaluation of the noradrenergic system in Parkinson's disease: an 11C-MeNER PET and neuromelanin MRI study. *Brain*. 2018;141(2):496-504. doi:10.1093/brain/awx348

16. Knudsen K, Fedorova TD, Hansen AK, et al. In-vivo staging of pathology in REM sleep behaviour disorder: a multimodality imaging case-control study. *The Lancet Neurology*. 2018;17(7):618-628. doi:10.1016/S1474-4422(18)30162-5

17. Braak E, Sandmann-Keil D, Rüb U, et al. alpha-synuclein immunopositive Parkinson's disease-related inclusion bodies in lower brain stem nuclei. *Acta Neuropathol*. 2001;101(3):195-201. doi:10/cgfbqf

18. Priovoulos N, Jacobs HIL, Ivanov D, Uludağ K, Verhey FRJ, Poser BA. High-resolution in vivo imaging of human locus coeruleus by magnetization transfer MRI at 3T and 7T. *NeuroImage*. 2018;168:427-436. doi:10.1016/j.neuroimage.2017.07.045

19. Liu KY, Marijatta F, Hämmerer D, Acosta-Cabronero J, Düzel E, Howard RJ. Magnetic resonance imaging of the human locus coeruleus: A systematic review. *Neuroscience & Biobehavioral Reviews*. 2017;83:325-355. doi:10.1016/j.neubiorev.2017.10.023

20. Betts MJ, Cardenas-Blanco A, Kanowski M, et al. Locus coeruleus MRI contrast is reduced in Alzheimer's disease dementia and correlates with CSF Aβ levels. *Alzheimer's & Dementia: Diagnosis, Assessment & Disease Monitoring*. 2019;11(1):281-285. doi:10.1016/j.dadm.2019.02.001

21. Betts MJ, Kirilina E, Otaduy MCG, et al. Locus coeruleus imaging as a biomarker for noradrenergic dysfunction in neurodegenerative diseases. *Brain*. 2019;142(9):2558-2571. doi:10.1093/brain/awz193

22. Nahimi A, Sommerauer M, Kinnerup MB, et al. Noradrenergic Deficits in Parkinson Disease Imaged with 11C-MeNER. *J Nucl Med*. 2018;59(4):659-664. doi:10.2967/jnumed.117.190975

23. Sommerauer M, Hansen AK, Parbo P, et al. Decreased noradrenaline transporter density in the motor cortex of Parkinson's disease patients: Cortical Noradrenaline Transporter. *Mov Disord*. 2018;33(6):1006-1010. doi:10.1002/mds.27411

24. Cheng H-C, Ulane CM, Burke RE. Clinical progression in Parkinson disease and the neurobiology of axons. *Ann Neurol*. 2010;67(6):715-725. doi:10.1002/ana.21995

25. Wong YC, Luk K, Purtell K, et al. Neuronal vulnerability in Parkinson disease: Should

the focus be on axons and synaptic terminals? *Mov Disord*. 2019;34(10):1406-1422. doi:10.1002/mds.27823

26. Grosch J, Winkler J, Kohl Z. Early Degeneration of Both Dopaminergic and Serotonergic Axons – A Common Mechanism in Parkinson's Disease. *Front Cell Neurosci*. 2016;10. doi:10.3389/fncel.2016.00293

27. Wihan J, Grosch J, Kalinichenko LS, Müller CP, Winkler J, Kohl Z. Layer-specific axonal degeneration of serotonergic fibers in the prefrontal cortex of aged A53T α-synuclein–expressing mice. *Neurobiology of Aging*. 2019;80:29-37. doi:10.1016/j.neurobiolaging.2019.03.014

28. Loughlin SE, Foote SL, Grzanna R. Efferent projections of nucleus locus coeruleus: Morphologic subpopulations have different efferent targets. *Neuroscience*. 1986;18(2):307-319. doi:10/bgb7fs

29. Mason ST, Fibiger HC. Regional topography within noradrenergic locus coeruleus as revealed by retrograde transport of horseradish peroxidase. *J Comp Neurol*. 1979;187(4):703-724. doi:10/ctxct7

30. Pickel VM, Segal M, Bloom FE. A radioautographic study of the efferent pathways of the nucleus locus coeruleus. *J Comp Neurol*. 1974;155(1):15-42. doi:10/dgs8dg

31. Satoh K, Tohyama M, Yamamoto K, Sakumoto T, Shimizu N. Noradrenaline innervation of the spinal cord studied by the horseradish peroxidase method combined with monoamine oxidase staining. *Exp Brain Res*. 1977;30(2-3):175-186. doi:10/b94ts9

32. German DC, Manaye KF, White CL, et al. Disease-specific patterns of locus coeruleus cell loss. *Ann Neurol*. 1992;32(5):667-676. doi:10.1002/ana.410320510

33. Postuma RB, Berg D, Stern M, et al. MDS clinical diagnostic criteria for Parkinson's disease: MDS-PD Clinical Diagnostic Criteria. *Mov Disord*. 2015;30(12):1591-1601. doi:10.1002/mds.26424

34. Tomlinson CL, Stowe R, Patel S, Rick C, Gray R, Clarke CE. Systematic review of levodopa dose equivalency reporting in Parkinson's disease: Systematic Review of LED Reporting in PD. *Mov Disord*. 2010;25(15):2649-2653. doi:10.1002/mds.23429

35. Goetz CG, Tilley BC, Shaftman SR, et al. Movement Disorder Society-sponsored revision of the Unified Parkinson's Disease Rating Scale (MDS-UPDRS): Scale presentation and clinimetric testing results: MDS-UPDRS: Clinimetric Assessment. *Mov Disord*. 2008;23(15):2129-2170. doi:10.1002/mds.22340

36. Yust-Katz S, Tesler D, Treves TA, Melamed E, Djaldetti R. Handedness as a predictor of side of onset of Parkinson's disease. *Parkinsonism Relat Disord*. 2008;14(8):633-635. doi:10/fskp9f

37. Sulzer D, Bogulavsky J, Larsen KE, et al. Neuromelanin biosynthesis is driven by excess cytosolic catecholamines not accumulated by synaptic vesicles. *Proc Natl Acad Sci U S A*.

2000;97(22):11869-11874. doi:10/bvfths

38. Zhang Y, Brady M, Smith S. Segmentation of brain MR images through a hidden Markov random field model and the expectation-maximization algorithm. *IEEE Trans Med Imaging*. 2001;20(1):45-57. doi:10/b647tb

39. Jenkinson M, Beckmann CF, Behrens TEJ, Woolrich MW, Smith SM. FSL. *NeuroImage*. 2012;62(2):782-790. doi:10/b9mzcr

40. Ehrminger M, Latimier A, Pyatigorskaya N, et al. The coeruleus/subcoeruleus complex in idiopathic rapid eye movement sleep behaviour disorder. *Brain*. 2016;139(4):1180-1188. doi:10.1093/brain/aww006

41. García-Lorenzo D, Longo-Dos Santos C, Ewenczyk C, et al. The coeruleus/subcoeruleus complex in rapid eye movement sleep behaviour disorders in Parkinson's disease. *Brain*. 2013;136(7):2120-2129. doi:10.1093/brain/awt152

42. Keren NI, Lozar CT, Harris KC, Morgan PS, Eckert MA. In vivo mapping of the human locus coeruleus. *NeuroImage*. 2009;47(4):1261-1267. doi:10.1016/j.neuroimage.2009.06.012

43. Yushkevich PA, Piven J, Hazlett HC, et al. User-guided 3D active contour segmentation of anatomical structures: Significantly improved efficiency and reliability. *NeuroImage*. 2006;31(3):1116-1128. doi:10/d585gp

44. Avants BB, Tustison NJ, Song G, Cook PA, Klein A, Gee JC. A reproducible evaluation of ANTs similarity metric performance in brain image registration. *NeuroImage*. 2011;54(3):2033-2044. doi:10/fvqcmw

45. Biondetti E, Gaurav R, Yahia-Cherif L, et al. Spatiotemporal changes in substantia nigra neuromelanin content in Parkinson's disease. *Brain*. 2020;143(9):2757-2770. doi:10.1093/brain/awaa216

46. Bates D, Mächler M, Bolker B, Walker S. Fitting Linear Mixed-Effects Models Using lme4. *Journal of Statistical Software*. 2015;67(1):1-48. doi:10/gcrnkw

47. Lenth RV, Buerkner P, Herve M, Love J, Riebl H, Singmann H. *Emmeans: Estimated Marginal Means, Aka Least-Squares Means*.; 2021. Accessed March 23, 2021. https://CRAN.R-project.org/package=emmeans

48. Dalrymple-Alford JC, MacAskill MR, Nakas CT, et al. The MoCA: Well-suited screen for cognitive impairment in Parkinson disease. *Neurology*. 2010;75(19):1717-1725. doi:10/cfrrfv

49. Pifl C, Kish SJ, Hornykiewicz O. Thalamic noradrenaline in Parkinson's disease: Deficits suggest role in motor and non-motor symptoms. *Mov Disord*. 2012;27(13):1618-1624. doi:10/f4f94w

50. Kish SJ, Shannak KS, Rajput AH, Gilbert JJ, Hornykiewicz O. Cerebellar Norepinephrine in Patients With Parkinson's Disease and Control Subjects. *Archives of Neurology*. 1984;41(6):612-614. doi:10/d7g97x

51. Gaspar P, Duyckaerts C, Alvarez C, Javoy-Agid F, Berger B. Alterations of dopaminergic and noradrenergic innervations in motor cortex in parkinson's disease. *Ann Neurol*. 1991;30(3):365-374. doi:10/bhx3gb

52. Braak H, Tredici KD, Rüb U, de Vos RAI, Jansen Steur ENH, Braak E. Staging of brain pathology related to sporadic Parkinson's disease. *Neurobiology of Aging*. 2003;24(2):197-211. doi:10.1016/S0197-4580(02)00065-9

53. Tagliaferro P, Burke RE. Retrograde Axonal Degeneration in Parkinson Disease. *JPD*. 2016;6(1):1-15. doi:10/f8w86q

54. O'Keeffe GW, Sullivan AM. Evidence for dopaminergic axonal degeneration as an early pathological process in Parkinson's disease. *Parkinsonism & Related Disorders*. 2018;56:9-15. doi:10/gh5vwz

55. Hansen AK, Knudsen K, Lillethorup TP, et al. In vivo imaging of neuromelanin in Parkinson's disease using 18F-AV-1451 PET. *Brain*. 2016;139(7):2039-2049. doi:10/gjx4b6

56. Bolam JP, Pissadaki EK. Living on the edge with too many mouths to feed: Why dopamine neurons die. *Mov Disord*. 2012;27(12):1478-1483. doi:10/ggrrqm

57. Surmeier DJ, Obeso JA, Halliday GM. Selective neuronal vulnerability in Parkinson disease. *Nat Rev Neurosci*. 2017;18(2):101-113. doi:10.1038/nrn.2016.178

58. Matsuda W, Furuta T, Nakamura KC, et al. Single Nigrostriatal Dopaminergic Neurons Form Widely Spread and Highly Dense Axonal Arborizations in the Neostriatum. *Journal of Neuroscience*. 2009;29(2):444-453. doi:10/fswnhr

59. Kebschull JM, Garcia da Silva P, Reid AP, Peikon ID, Albeanu DF, Zador AM. High-Throughput Mapping of Single-Neuron Projections by Sequencing of Barcoded RNA. *Neuron*. 2016;91(5):975-987. doi:10/f83gw6

60. Kordower JH, Olanow CW, Dodiya HB, et al. Disease duration and the integrity of the nigrostriatal system in Parkinson's disease. *Brain*. 2013;136(8):2419-2431. doi:10/f45s8p

61. Monje MHG, Blesa J, García-Cabezas MÁ, Obeso JA, Cavada C. Changes in Thalamic Dopamine Innervation in a Progressive Parkinson's Disease Model in Monkeys. *Mov Disord*. 2020;35(3):419-430. doi:10/gjzbgg

62. Mulcahy P, Walsh S, Paucard A, Rea K, Dowd E. Characterisation of a novel model of Parkinson's disease by intra-striatal infusion of the pesticide rotenone. *Neuroscience*. 2011;181:234-242. doi:10/d7jmwg

63. Bourdenx M, Dovero S, Engeln M, et al. Lack of additive role of ageing in nigrostriatal neurodegeneration triggered by α-synuclein overexpression. *Acta Neuropathol Commun*. 2015;3(1):46. doi:10/gb9tk4

64. Arcuri L, Viaro R, Bido S, et al. Genetic and pharmacological evidence that endogenous nociceptin/orphanin FQ contributes to dopamine cell loss in Parkinson's disease. *Neurobiology of*

Disease. 2016;89:55-64. doi:10/gjzbgj

65. Pérez-Taboada I, Alberquilla S, Martín ED, et al. Diabetes Causes Dysfunctional Dopamine Neurotransmission Favoring Nigrostriatal Degeneration in Mice. *Mov Disord*. 2020;35(9):1636-1648. doi:10/gjzbgk

66. Abeliovich A, Gitler AD. Defects in trafficking bridge Parkinson's disease pathology and genetics. *Nature*. 2016;539(7628):207-216. doi:10/f895x6

67. Goldstein DS. The "Sick-but-not-Dead" Phenomenon Applied to Catecholamine Deficiency in Neurodegenerative Diseases. *Semin Neurol*. 2020;40(05):502-514. doi:10/gjzbgm

68. Saari L, Kivinen K, Gardberg M, Joutsa J, Noponen T, Kaasinen V. Dopamine transporter imaging does not predict the number of nigral neurons in Parkinson disease. *Neurology*. 2017;88(15):1461-1467. doi:10/f9zq58

69. Kuya K, Shinohara Y, Miyoshi F, Fujii S, Tanabe Y, Ogawa T. Correlation between neuromelanin-sensitive MR imaging and 123I-FP-CIT SPECT in patients with parkinsonism. *Neuroradiology*. 2016;58(4):351-356. doi:10/f8hdbq

70. Kraemmer J, Kovacs GG, Perju-Dumbrava L, Pirker S, Traub-Weidinger T, Pirker W. Correlation of striatal dopamine transporter imaging with post mortem substantia nigra cell counts: Correlation of DAT Imaging with SN Cell Counts. *Mov Disord*. 2014;29(14):1767-1773. doi:10/f6r78c

71. Colloby SJ, McParland S, O'Brien JT, Attems J. Neuropathological correlates of dopaminergic imaging in Alzheimer's disease and Lewy body dementias. *Brain*. 2012;135(9):2798-2808. doi:10/gjzbgz

72. Isaias IU, Trujillo P, Summers P, et al. Neuromelanin Imaging and Dopaminergic Loss in Parkinson's Disease. *Front Aging Neurosci*. 2016;8:196. doi:10/gjvpqn

73. Martín-Bastida A, Lao-Kaim NP, Roussakis AA, et al. Relationship between neuromelanin and dopamine terminals within the Parkinson's nigrostriatal system. *Brain*. 2019;142(7):2023-2036. doi:10.1093/brain/awz120

74. Uematsu A, Tan BZ, Ycu EA, et al. Modular organization of the brainstem noradrenaline system coordinates opposing learning states. *Nat Neurosci*. 2017;20(11):1602-1611. doi:10/gbxg95

75. Schwarz LA, Miyamichi K, Gao XJ, et al. Viral-genetic tracing of the input–output organization of a central noradrenaline circuit. *Nature*. 2015;524(7563):88-92. doi:10/f7mj5t

76. Redgrave P, Rodriguez M, Smith Y, et al. Goal-directed and habitual control in the basal ganglia: implications for Parkinson's disease. *Nat Rev Neurosci*. 2010;11(11):760-772. doi:10/c53hd9

77. Li Y, Wang C, Wang J, et al. Mild cognitive impairment in de novo Parkinson's disease: A neuromelanin MRI study in locus coeruleus. *Mov Disord*. 2019;34(6):884-892. doi:10/gghdtg

78. Borghammer P. The α-Synuclein Origin and Connectome Model (SOC Model) of Parkinson's Disease: Explaining Motor Asymmetry, Non-Motor Phenotypes, and Cognitive Decline. *J Parkinsons Dis*. 2021;11(2):455-474. doi:10/gjtfbb

79. Ye R, Rua C, O'Callaghan C, et al. An in vivo probabilistic atlas of the human locus coeruleus at ultra-high field. *Neuroimage*. 2021;225:117487. doi:10/gjs8mx

80. Mäki-Marttunen V, Espeseth T. Uncovering the locus coeruleus: Comparison of localization methods for functional analysis. *NeuroImage*. 2021;224:117409. doi:10.1016/j.neuroimage.2020.117409

81. Ohtsuka C, Sasaki M, Konno K, et al. Changes in substantia nigra and locus coeruleus in patients with early-stage Parkinson's disease using neuromelanin-sensitive MR imaging. *Neurosci Lett*. 2013;541:93-98. doi:10/f4wh3v

82. Wang J, Li Y, Huang Z, et al. Neuromelanin-sensitive magnetic resonance imaging features of the substantia nigra and locus coeruleus in de novo Parkinson's disease and its phenotypes. *European Journal of Neurology*. 2018;25(7):949-e73. doi:10/gdbtcw

83. Ariz M, Abad RC, Castellanos G, et al. Dynamic Atlas-Based Segmentation and Quantification of Neuromelanin-Rich Brainstem Structures in Parkinson Disease. *IEEE Trans Med Imaging*. 2019;38(3):813-823. doi:10/gjzbj3

84. Simões RM, Castro Caldas A, Grilo J, et al. A distinct neuromelanin magnetic resonance imaging pattern in parkinsonian multiple system atrophy. *BMC Neurol*. 2020;20(1):432. doi:10/gjzbkf

85. Horsager J, Andersen KB, Knudsen K, et al. Brain-first versus body-first Parkinson's disease: a multimodal imaging case-control study. *Brain*. 2020;143(10):3077-3088. doi:10.1093/brain/awaa238

86. Liu KY, Acosta-Cabronero J, Cardenas-Blanco A, et al. In vivo visualization of age-related differences in the locus coeruleus. *Neurobiology of Aging*. 2019;74:101-111. doi:10.1016/j.neurobiolaging.2018.10.014

87. Wilson AA, Johnson DP, Mozley D, et al. Synthesis and in vivo evaluation of novel radiotracers for the in vivo imaging of the norepinephrine transporter. *Nucl Med Biol*. 2003;30(2):85-92. doi:10/dxvszw

88. Ghose S, Fujita M, Morrison P, et al. Specific in vitro binding of (S,S)-[3H]MeNER to norepinephrine transporters. *Synapse*. 2005;56(2):100-104. doi:10/fnfch2

89. Schou M, Halldin C, Sóvágó J, et al. Specific in vivo binding to the norepinephrine transporter demonstrated with the PET radioligand, (S,S)-[11C]MeNER. *Nuclear Medicine and Biology*. 2003;30(7):707-714. doi:10.1016/S0969-8051(03)00079-9

Figure legends

Figure 1: Schematic depiction of the processing pipeline. TSE images of healthy controls (HC) and Parkinson's disease (PD) patients in native space were bias-field corrected. The locus coeruleus (LC) was manually segmented to extract its volume (red box) and to build a sample-specific probabilistic map, which was then used to extract the mean voxel intensity along the full extent of the LC and additionally of its parts subdivided along the rostro-caudal axis (orange box). In a second approach, the voxels with the highest intensity within larger "LC searching volumes of interest (VOIs)" were identified, again for the full LC (12 connected voxels, 10 independent voxels) and along the rostro-caudal axis (5 independent voxels of rostral, middle, and caudal part) (blue box). Pontine VOIs are shown in white.
Abbreviations: ANTs = Advanced Normalization Tools, FSL = FMRIB Software Library, FAST = FMRIB's Automated Segmentation Tool, TSE = turbo spin-echo.

Figure 2: Four different MRI neuromelanin assessments of the locus coeruleus. Dot plots showing individual mean voxel intensity of the 12 connected voxels with the highest intensity, mean voxel intensity of the 10 independent voxels with the highest intensity within "searching volumes of interest", and mean voxel intensity extracted using a study-specific probabilistic map in healthy controls (HC, black) and Parkinson's disease patients (PD, grey). Right panel: Cumulative bilateral locus coeruleus (LC) volumes in mm^3 derived from manual LC segmentations of individual subjects. Horizontal lines represent the mean of each group (*: $p < 0.05$, ***: $p < 0.001$, ****: $p < 0.0001$).

Figure 3: MRI neuromelanin contrast along the rostro-caudal axis of the locus coeruleus assessed using two different methods. Dot plots depicting **(A)** individual mean voxel intensity of healthy controls (HC, dark colors) and Parkinson's disease patients (PD, light colors) extracted from neuromelanin-sensitive MRI images using a probabilistic map subdivided in rostral (blue), middle (pink), and caudal (yellow) parts and **(B)** individual mean voxel intensity of the five independent voxels with the highest intensity within "searching volumes of interest" subdivided along the rostro-caudal axis of the locus coeruleus. Horizontal lines represent the mean of each

group. Colour-coding is analogous to rostro-caudal delineations of the locus coeruleus as in figure 1 (*: $p < 0.05$, **: $p < 0.01$, ****: $p < 0.0001$).

Figure 4: MRI neuromelanin contrast of the locus coeruleus in Parkinson's disease patients differentiating between most and least affected side. Dot plots showing **(A)** individual mean voxel intensity of the entire probabilistic map and **(B)** subdivided along the rostro-caudal axis of the locus coeruleus. Horizontal lines represent the mean of each side. Color-coding for the different subdivision is analogous to rostro-caudal delineations of the locus coeruleus as in figures 1 and 3 (*: $p < 0.05$).

Figure 5: ^{11}C-MeNER DVRs of healthy controls and Parkinson's disease patients. Averaged ^{11}C-MeNER distribution volume ratios (DVR) in noradrenaline transporter rich regions of healthy controls (HC, black) and Parkinson's disease patients (PD, grey). Horizontal lines represent the mean of each group (*: $p < 0.05$, **: $p < 0.01$, ***: $p < 0.001$, ****: $p < 0.0001$).

Figure 6: Correlation of ^{11}C-MeNER DVR and MRI neuromelanin contrast of the locus coeruleus extracted from the study-specific probabilistic map. Scatterplots showing ^{11}C-MeNER DVR and mean voxel intensities for Parkinson's disease patients (PD, grey) and healthy controls (HC, black). The correlation was computed using Pearson's correlation coefficient considering partial correlations with age, gender, scanner type, and MoCA score. Values in brackets denote correlation coefficients and p-values irrespective of these covariates.

Figure 7: Normalized ratio of ^{11}C-MeNER DVRs in noradrenaline transporter-rich regions to MRI neuromelanin contrast of the locus coeruleus extracted from the study-specific probabilistic map. Ratios were calculated intraindividually for healthy controls (HC, black) and Parkinson's disease patients (PD, grey) and normalized to the HC mean per region. Horizontal lines represent the mean of each group (= 1 for HC in all regions) (*: $p < 0.05$, ***: $p < 0.001$).

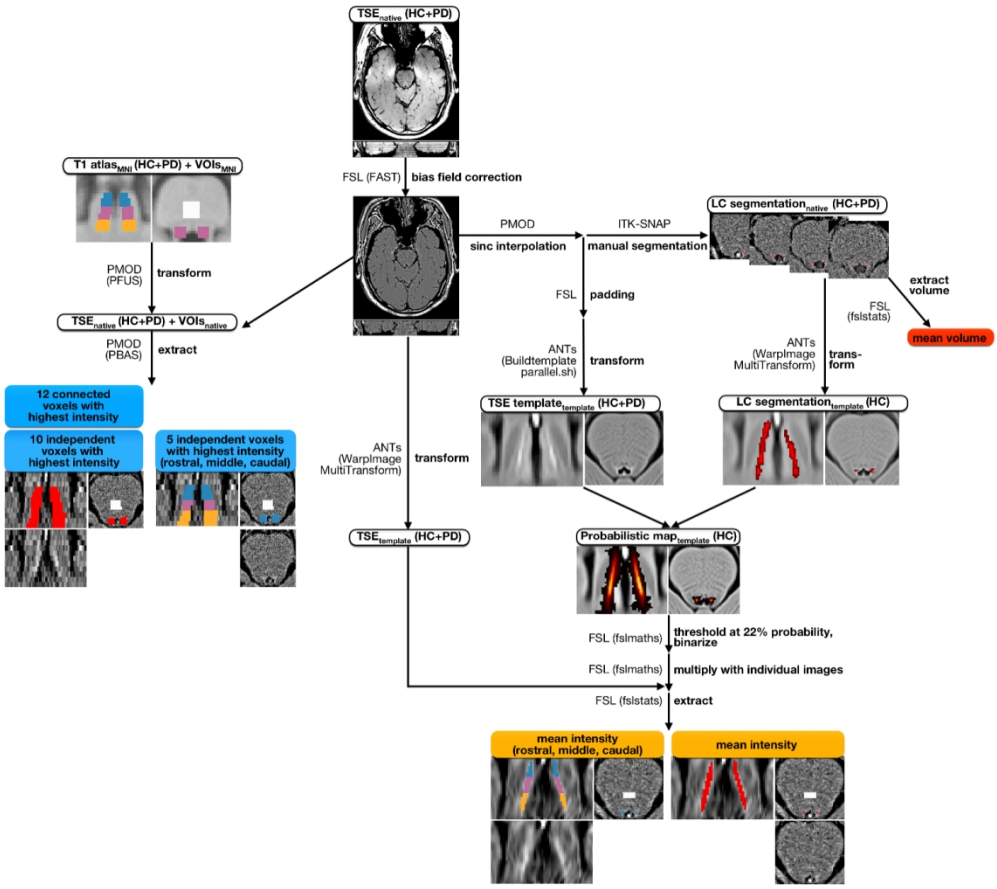

Figure 1

261x253mm (151 x 151 DPI)

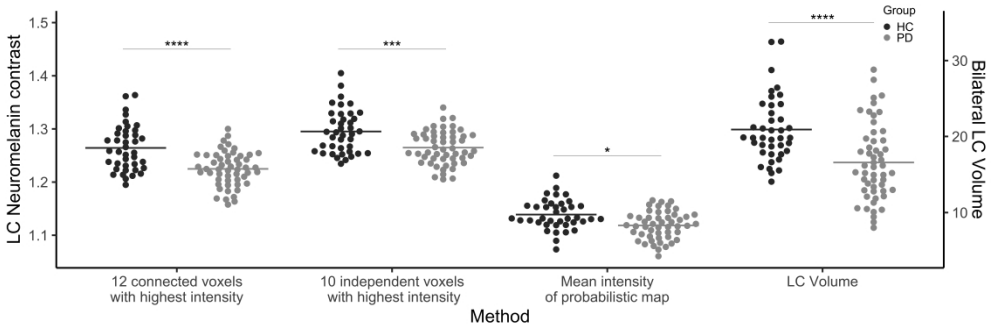

Figure 2

3749x1249mm (72 x 72 DPI)

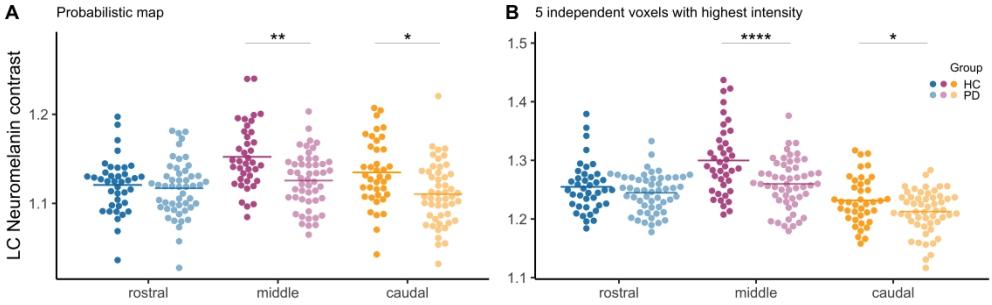

Figure 3

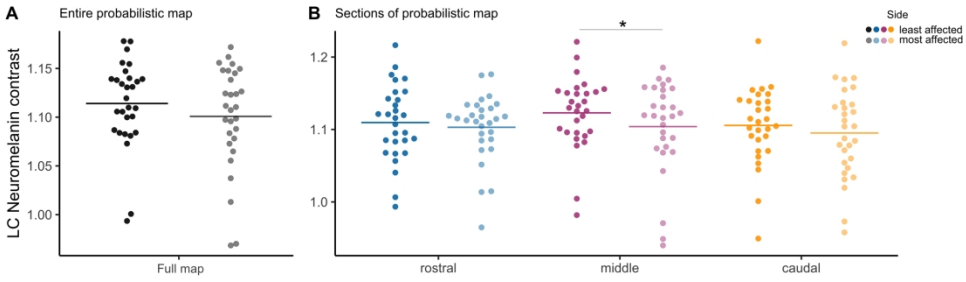

Figure 4

184x56mm (300 x 300 DPI)

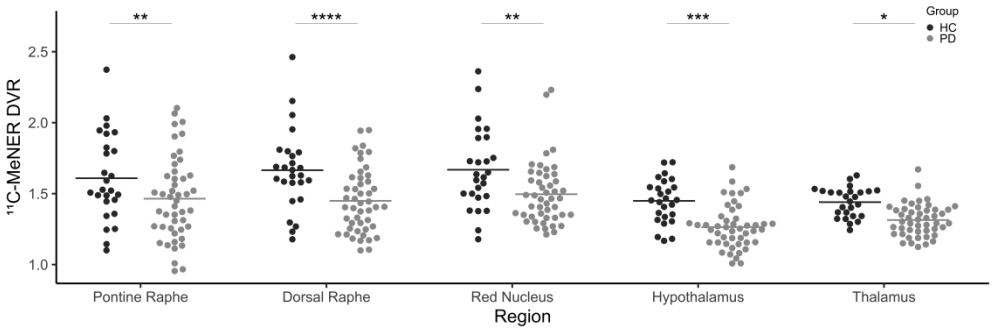

Figure 5

3749x1249mm (72 x 72 DPI)

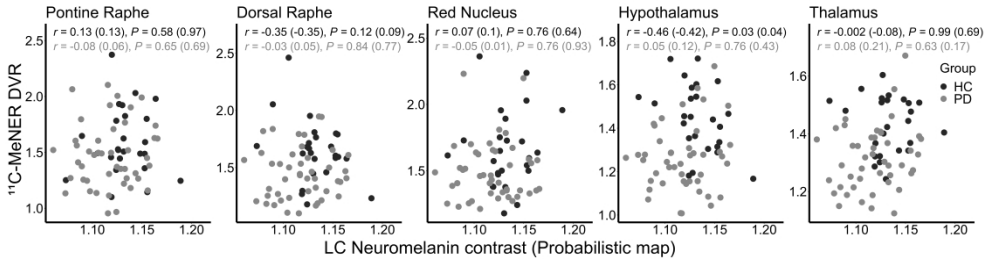

Figure 6

3374x874mm (72 x 72 DPI)

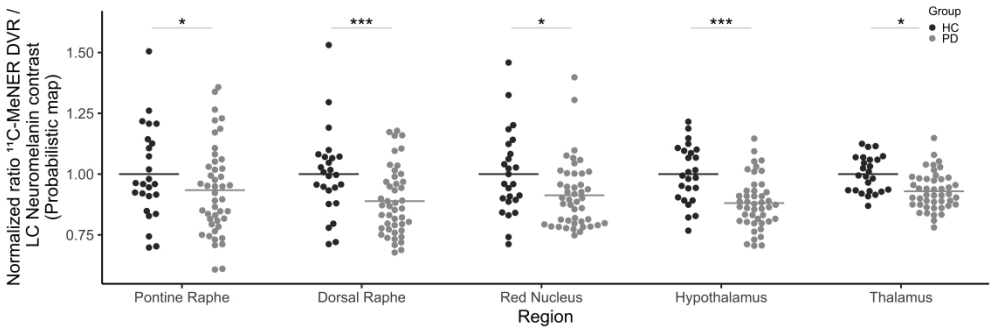

Figure 7

Table 1 Demographic and clinical characteristics of included subjects

	all HC (n = 39)	all PD (n = 50)	*p*	HC (MRI + PET) (n = 26)	PD (MRI + PET) (n = 47)	*p*
Age [years]	66.0 ± 6.8	66.2 ± 8.2	0.652[a]	66.5 ± 6.8	66.2 ± 8.4	0.849[a]
Sex [male/female]	17/22	35/15	**0.022**[b]	13/13	32/15	**0.020**[b]
MoCA	27.8 ± 2.1	26.6 ± 2.2	**0.016**[a]	27.4 ± 2.2	26.8 ± 2.2	0.186[a]
GDS-15	0.3 ± 0.7	1.1 ± 1.6	**<0.01**[a]	0.3 ± 0.5	1.0 ± 1.6	**0.041**[a]
Difference between acquisition of PET and MRI [days]	-	-	-	45.9 ± 104.8	41.2 ± 111.6	0.784[a]
Disease duration [years]	-	4.8 ± 3.7	-	-	5.0 ± 3.7	-
Hoehn & Yahr stage	-	2.4 ± 0.6	-	-	2.4 ± 0.5	-
Most affected side [left/right/indifferent]	-	7/19/24	-	-	7/19/21	-
LEDD [mg]	-	554.5 ± 357.2	-	-	540.2 ± 364.1	-
treatment-naïve [n]	-	1	-	-	1	-
MDS-UPDRS III[c]	-	35.4 ± 10.7	-	-	34.3 ± 11.1	-

Values depicted as mean ± standard deviation. Bold numbers indicate significant differences. GDS-15 = 15-item Geriatric Depression Scale, HC = healthy control subjects, LEDD = Levodopa-equivalent daily dose, MoCA = Montreal Cognitive Assessment, PD = Parkinson's disease patients, PET = Positron emission tomography, MDS-UPDRS III = Movement Disorder Society – Unified Parkinson's disease Rating Scale part III.

[a]Non-parametric Mann-Whitney-Test.

[b]Chi-square test.

[c]In a subset of 25 patients, the Unified Parkinson's disease Rating Scale part III (UPDRS III) was used. Values were converted to the MDS-UPDRS III system using the approach suggested by the Movement Disorder Society.[30]